JOURNAL OF GEOPHYSICAL RESEARCH, VOL. 113, A07S27, doi:10.1029/2007JA012685, 2008

Observations of an active thin current sheet

A. Runov,[1,2] W. Baumjohann,[1] R. Nakamura,[1] V. A. Sergeev,[3] O. Amm,[4] H. Frey,[5] I. Alexeev,[6] A. N. Fazakerley,[6] C. J. Owen,[6] E. Lucek,[7] M. André,[8] A. Vaivads,[8] I. Dandouras,[9] and B. Klecker[10]

Received 26 July 2007; revised 27 February 2008; accepted 26 March 2008; published 15 July 2008.

[1] We analyze observations of magnetotail current sheet dynamics during a substorm between 2330 and 2400 UT on 28 August 2005 when Cluster was in the plasma sheet at [−17.2, −4.49, 0.03] R_E (GSM) with the foot points near the IMAGE ground-based network. Observations from the Cluster spacecraft, ground-based magnetometers, and the IMAGE satellite showed that the substorm started in a localized region near midnight, expanding azimuthally. A thin current sheet with a thickness of less than 900 km and current density of about 30 nA/m^2 was observed during 5 min around the substorm onset. The thinning of the current sheet was accompanied by tailward plasma flow at a velocity of −700 km/s and subsequent reversal to earthward flow at $V_x \approx 500$ km/s coinciding with a B_z turning from −5 to +10 nT. The analysis of magnetic and electric fields behavior and particle distributions reveals signatures of impulsive (with ∼1 min timescale) activations of the thin current sheet. These observations were interpreted in the framework of transient reconnection, although the data analysis reveals serious disagreements with the classical 2.5-D X line model.

Citation: Runov, A., et al. (2008), Observations of an active thin current sheet, *J. Geophys. Res.*, *113*, A07S27, doi:10.1029/2007JA012685.

1. Introduction

[2] Formation and instability of thin current sheets (TCS) in the magnetotail are recognized to be key processes during substorms [e.g., *Baumjohann et al.*, 2007, and references therein]. It is established that TCSs may thin down to about ion inertial scale c/ω_{pi} during the late growth phase of substorms [e.g., *Asano et al.*, 2004], during high-speed flow intervals [e.g., *Nakamura et al.*, 2002], and in reconnection sites [e.g., *Runov et al.*, 2003; *Nakamura et al.*, 2006]. TCSs are the active regions, in which microinstabilities may lead to explosive release of the magnetic energy resulting in particle acceleration.

[3] The key element of the energy conversion in TCS is a breakdown of the frozen-in condition, under which the plasma and magnetic field are moving together [see, e.g., *Baumjohann and Treumann*, 1996]. Magnetic reconnection, which recognized to be the most effective way of the energy conversion, implies a violation of the frozen-in condition within a diffusion region with the scale of c/ω_{pi} (see *Birn and Priest* [2007] for details). In TCSs with a thicknesses comparable to c/ω_{pi}, ions become unmagnetized and move separately from electrons, which leads to a negative charging of such sheets and generation of Hall currents [*Sonnerup*, 1979; *Treumann et al.*, 2006]. Negative charging of the inner part of a TCS leads to appearance of the electric field, directed toward the neutral sheet. The component of the electric field, normal to the thin current sheet, was observed at the magnetopause [e.g., *Vaivads et al.*, 2004] and in the magnetotail [*Wygant et al.*, 2005; *Borg et al.*, 2005; *Eastwood et al.*, 2007]. The reconnection scenario includes a formation of one or several magnetic X lines with the quadrupolar Hall magnetic field coinciding with the reversal of high-speed bulk flow. The X line magnetic structure with a quadrupolar field was observed during reconnection events on magnetopause [e.g., *Vaivads et al.*, 2004], in the distant [*Oieroset et al.*, 2001] and near-Earth magnetotail [*Nagai et al.*, 1998, 2003; *Runov et al.*, 2003; *Sergeev et al.*, 2007].

[4] Alternatively, bulk flow reversals in TCSs may be caused by generation of local inductive electric field during a cross-tail current disruption (CD) because of current driven instabilities [e.g., *Lui*, 1996; *Lui et al.*, 2006] or by ballooning instability [e.g. *Roux et al.*, 1991; *Bhattacharjee et al.*, 1998; *Pritchett and Coronoti*, 1999]. Regardless to the instability type, the CD is essentially 3-D process,

[1]Space Research Institute, Austrian Academy of Sciences, Graz, Austria.
[2]Now at Institute of Geophysics and Planetary Physics, University of California, Los Angeles, California, USA.
[3]Institute of Physics, St. Petersburg State University, St. Petersburg, Russia.
[4]Finnish Meteorological Institute, Helsinki, Finland.
[5]Space Sciences Laboratory, University of California, Berkeley, California, USA.
[6]Mullard Space Science Laboratory, University College London, Dorking, UK.
[7]Space and Atmospheric Physics Group, Blackett Laboratory, Imperial College, London, UK.
[8]Swedish Institute of Space Physics, Uppsala, Sweden.
[9]CESR/CNRS, Toulouse, France.
[10]MPE, Garching, Germany.

0148-0227/08/2007JA012685$09.00

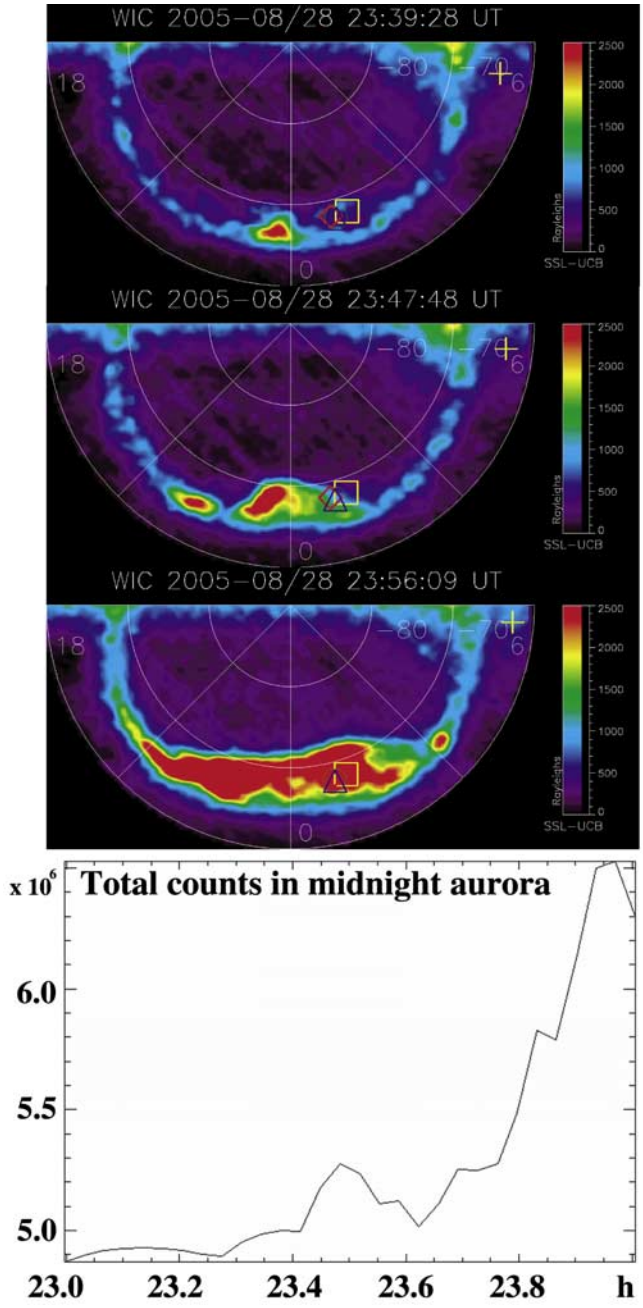

Figure 1. (top) Set of auroral images, obtained by IMAGE/Wideband Imaging Camera during 2339–2400 UT on 28 August 2005, with the Cluster spacecraft foot points computed using the T96 model. (bottom) Brightness of the midnight aurora.

including dynamics in cross-tail direction. Particularly, the drift ballooning mode produces quasiperiodic variation of the electric and magnetic fields with the azimuthal wave number $k_y \gg (k_x, k_z)$. Observations of CD in the magnetotail at $R \approx -8$ R_E showed variations of the magnetic field and energetic ion flux at timescale of 10–100 s [*Chen et al.*, 2003]. CD-related turbulence may sufficiently suppress the electric conductivity of plasma resulting with breakdown of the frozen-in condition in a region with a scale larger than c/ω_{pi} [*Lui et al.*, 2007].

[5] In the present paper, we report on Cluster observations of the thin current sheet with ion flow reversal during a substorm on 28 August 2005. In the 2005 tail season, the Cluster spacecraft formed a large-scale (~2 R_E) triangle in the equatorial (*XY*, GSM) plane, with a pair of closely situated (~900 km separation) probes in the most earthward node [see, e.g., *Sergeev et al.*, 2007]. For the 28 August 2005 event, such configuration enables to monitor the thin current sheet interior, outer plasma sheet, and the PSBL simultaneously. We study magnetic and electric field and particle data, examining the frozen-in condition, temporal and spatial scales of the thin current sheet activity.

2. Event Overview

[6] We discuss the magnetotail current sheet dynamics during 2300–2400 UT, 28 August 2005. The event continued until about 0100 UT on the next day.

[7] Southward tuning of the IMF was detected by the WIND spacecraft, located at [225.7, −99.3, 19.7] R_E, at 2200 UT (not shown). Between 2258 and 2306 UT, the IMF experienced a northward excursion, then stayed southward, fluctuating between −2 and −4 nT. The IMF B_y fluctuated at the level of −3 nT with a brief drop down to zero at about 2330 UT. The solar wind dynamic pressure was stable at about 1.45 nPa during 2300–2400 UT.

[8] Figure 1 presents a set of auroral images, obtained by IMAGE/Wideband Imaging Camera, showing the auroral substorm development between 2339 and 2400 UT and the Cluster foot point, calculated using the T96 model [*Tsyganenko*, 1995]. The bottom panel shows the evolution of the aurora brightness in the midnight sector during 2300–2400 UT. A local enhancement of aurora was detected between 2312 and 2338 UT. The major expansion phase started at around 2339 UT with an activation near the midnight meridian, westward of the Cluster foot point location.

[9] Figure 2 shows the evolution of the ionospheric equivalent current, calculated from the the IMAGE magnetometer network data for the interval between 2300 UT on 28 August and 0100 UT on 29 August. Cluster was in a conjunction with the IMAGE network during 2200–2400 UT. The equatorward motion of the enhanced ionospheric current, indicating a growth phase [e.g., *Pellinen et al.*, 1982], began at ~2312 UT and continued until ~2348 UT with two short poleward expansions at 2330 and 2336 UT. The major poleward expansion at IMAGE/Cluster location (~0050 MLT) started at 2348 UT on 28 August and continued until 0100 UT on 29 August.

[10] Figure 3 shows a summary plot of the magnetic field from the Cluster Fluxgate Magnetometer (FGM) [*Balogh et al.*, 2001] and the ion velocity from the Cluster Ion Spectrometry (CIS) [*Rème et al.*, 2001] experiment at the four Cluster spacecraft. Plotting the FGM data, we use a cartesian coordinate system, rotated by 16.4° with respect to GSM around the *Z* axis, to diminish the flaring effect. The angle was obtained from a linear regression between B_x and B_y. Minimum variance analysis (MVA), applied to the magnetic field during the entire interval, yields the same result. Cluster spacecraft positions were (GSM, R_E) [−17.2, −4.48, 0.03] (C1), [−17.8, −3.17, 0.37] (C2), [−16.6, −3.36, 0.11] (C3), and [−16.5, −3.38, 0.25] (C4).

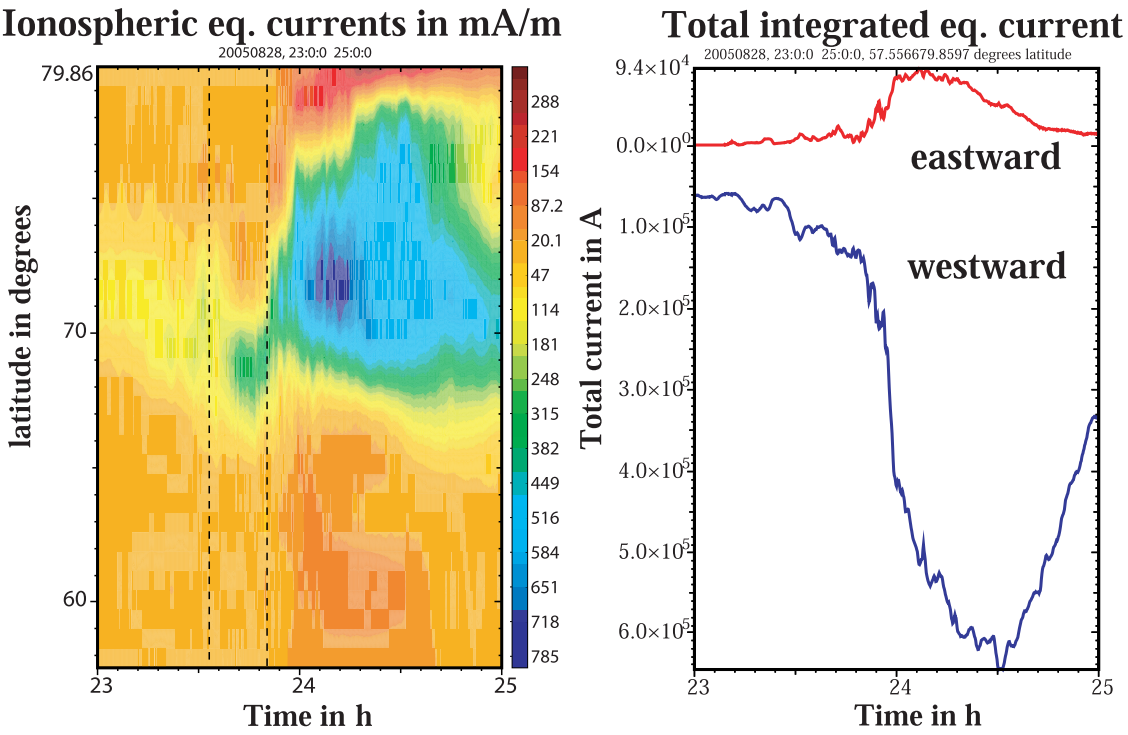

Figure 2. Equivalent ionospheric current density (2-D) and total integrated equivalent currents (1-D), calculated from IMAGE ground-based magnetometers array data during 2300–0100 UT on 28–29 August 2005. Dashed vertical lines indicate the interval of TCS and the flow reversal observed by Cluster.

Thus, in the $(XY)_{GSM}$ plane, Cluster formed a triangle with the lengths of 9000 km, with the C3/C4 pair in the earthward node. C1 is in the dawnward node, and C2 the tailward one. C3 and C4 are separated by 900 km (Figures 3a–3c). This configuration allows to probe the fluid ($\geq R_E$) and the ion scale (of 2–3 ion inertial lengths) simultaneously. The Cluster configuration in the modified coordinate system is shown in Figures 3a–3c).

[11] Between 2300 and 2312 UT the magnetic field at Cluster was oscillating with the four traces close together. After 2312 UT, during the substorm growth phase (see Figure 2), Cluster/FGM started to detect an enhancement of the magnetic field gradient: the differences between the C2, C3/C4, and C1 B_x traces (Figure 3d) became significant. The difference between B_x at C3 and C4 is used to estimate the current density in the plasma sheet (Figure 3g). It increased drastically at 2337 UT and stayed between 20 and 30 nA/m^2 until 2342 UT. During this interval, C3 detected B_x fluctuating at about −15 nT, while B_x at C4 is of 15–20 nT. Thus, Cluster encountered a thin current sheet with a thickness of about 900 km (distance between C3 and C4). The ion bulk velocity (Figures 3h and 3i), obtained by Cluster/CIS at C1, C3 and C4, was tailward and duskward flow ($V_x \sim -600$ km/s, $V_y \sim 200$ km/s at C3 and $V_y \sim 500$ km/s at C4) during 2336–2341 UT and reversed to earthward and duskward ($V_x \sim 500$ km/s, $V_y \sim 200$ km/s) at 2341 UT at C3/C4 and at 2344 UT at C1. Note that the duskward flow is larger at C4 and has a maximum at the V_x reversal. This duskward flow is due to remote sensing of the TCS by high-energy protons [e.g., *Wilber et al.*, 2004]. The difference in the four B_x traces disappeared at about 2347:45 UT, when the magnetic field fluctuations increased in amplitude up to 15 nT ($>\langle B\rangle$). The ion bulk velocity was fluctuating between 500 and 900 km/s.

3. Detailed Analysis

[12] In this section we discuss the observations during 2333–2347 UT (boxed by dashed lines in Figures 2 and 3), when Cluster encountered the TCS with the flow reversal from tailward to earthward, in detail. Figure 4 presents a summary plot of Cluster measurements during this interval: the history of the B_x, B_y, and B_z components in the modified GSM coordinate system (the "′" mark is omitted further on), the estimate of the cross-tail current density $\Delta B_{x34}/\Delta Z_{34}$, the X component of the ion bulk velocity; energy-time spectra at C1, C3 and C4 for earthward and tailward streaming ions, and, finally, the omnidirectional electron energy-time spectrum, obtained by the Plasma Electron And Current Experiment (PEACE) [*Johnstone et al.*, 1997] at C2.

[13] At the beginning of this interval all four spacecraft were in the southern half of the plasma sheet at B_x levels of −7 nT (C2) and of −15 nT (C1, C3 and C4). Between 2334 and 2338 UT, first C2 then C4, and, finally, C3 crossed the current sheet, entering to the northern half of the plasma sheet, while C1 stayed in the southern half, at the B_x level of −15 nT. The B_x traces at all four probes are similar in shape during 2334–2338 UT. The average B_y and B_z components (modified GSM) in the neutral sheet ($|B_x| < 3$ nT) were −5.9 ± 1.7 nT and 3.8 ± 1.2 nT, respectively, similar at the three probes, crossing the current sheet. The best correlation of the B_x traces was found at lag

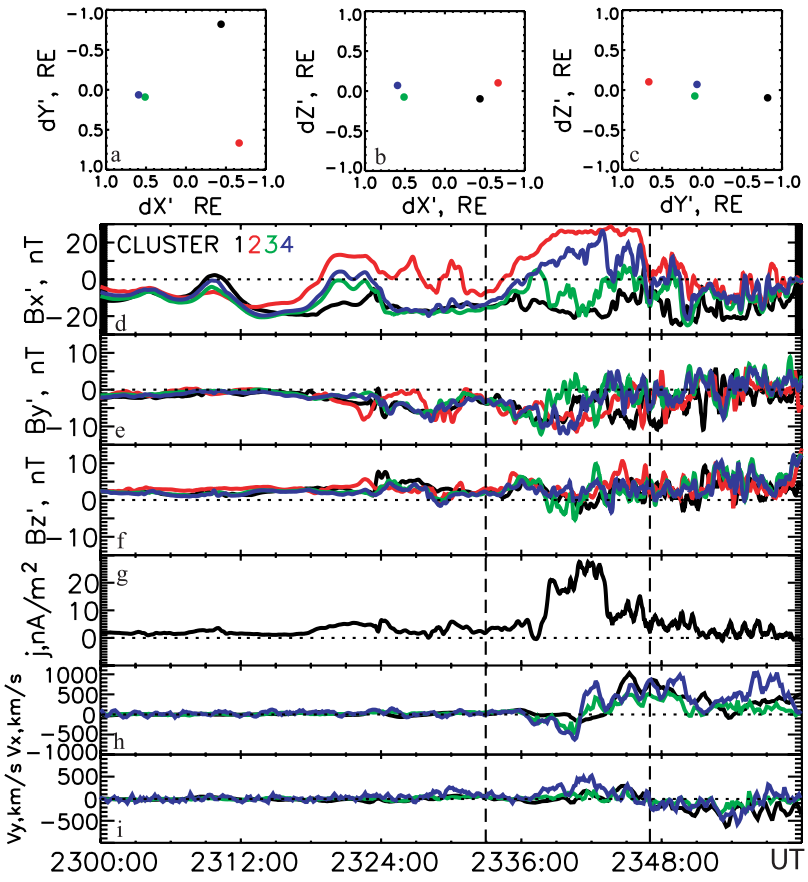

Figure 3. Cluster observations during 2300–2400 UT, on 28 August 2005. (a–c) Cluster configuration in the modified GSM frame (rotated by 16.4° around Z). (d–f) Magnetic field components from Cluster/FGM in the modified GSM frame. (g) The current density estimate, $j = \mu_0^{-1}\, dBx_{34}/dZ_{34}$. (h and i) X and Y components of the ion bulk velocity at C1 and C3 (CIS–ion Composition Distribution Function Analyzer (CODIF)) and at C4 (CIS–Hot Ion Analyzer (HIA)).

times dt = [99, 94, 72] s with respect to the trace at C2. Thus, the current sheet moved southward and dawnward at a velocity of 50 km/s with respect to the spacecraft quartet.

[14] Between 2337:30 and 2338:30 UT, C3 crossed the current sheet starting at 8 nT and ending at −14 nT, while C4, separated by ∼900 km in the Z direction, detected B_x fluctuating between 8 and 12 nT. This corresponds to a jump of the current density up to 20 nA/m^2. C3 stayed mainly in the southern half of the current sheet detecting $-21 < B_x \leq 0$ nT until 2343:30 UT, while C4 stayed in the northern half at $3 \leq B_x \leq 27$ nT. Although the magnetic field fluctuated with amplitude up to 15 nT, the current density stayed varying between 20 and 30 nA/m^2. Thus, during about 5 min the C3/C4 pair stayed in TCS, with a thickness of less than 900 km (C3/C4 separation). The enhancement of the cross-tail current density coincided with the aurora brightening as detected by IMAGE at 2339:38 UT (Figure 1). It should be noted, that C1 and C4 detected $B_y \approx -10$ nT between 2338 and 2341 UT. Hence, the estimated current density includes significant component parallel to the magnetic field.

[15] The C3 crossing of the TCS at 2338 UT may be used to determine the TCS orientation. MVA of the magnetic filed at C3 for 2337:41–2338:21 UT yields eigenvalues λ = [53.5, 1.40, 0.12], and a normal vector $\mathbf{N}$ = [−0.2, 0.07, 0.98]. Thus the TCS geometry was close to nominal with the normal directed along Z_{GSM}. The average normal component of the magnetic field in the neutral sheet was 1.40 ± 0.96 nT, i.e., smaller than during the preceding crossing of the thicker current sheet. C3 and C4 stayed in southern and northern halves of the current sheet, respectively, while C1 was more to the south and ∼0.8 R_E dawnward in the plasma sheet (PS). C2 exited the plasma sheet, detecting a drop of the ∼1 keV electron flux at about 2338:30 UT and stayed in the PSBL between 2338:30 and 2341:00 UT and in the northern lobe during 2341–2343 UT.

[16] At about 2336 UT, the CIS instruments at C3 and C4 started to detect the flux of tailward streaming ions at energies >5 keV (Figure 4). After 2341 UT (short-dashed line in Figure 4) the direction of the ion streaming changed to earthward. The ion bulk velocity reversed from −500 km/s to ∼500 km/s at C3 and to ∼800 km/s at C4. At C1, the energy of tailward and earthward streaming ions decreased between 2338 and 2340:30 UT. At 2340:30 UT, C1 detected a tailward streaming high-energy ion population, coexisting with a nearly isotropic lower-energy one. These two populations are seen in the ion distribution function (Figure 5, top) where $V_{\|}$ is the velocity, parallel to the magnetic field averaged over three spins, [−15.2, −7.3, −3.1] nT, and $V_{\perp}$

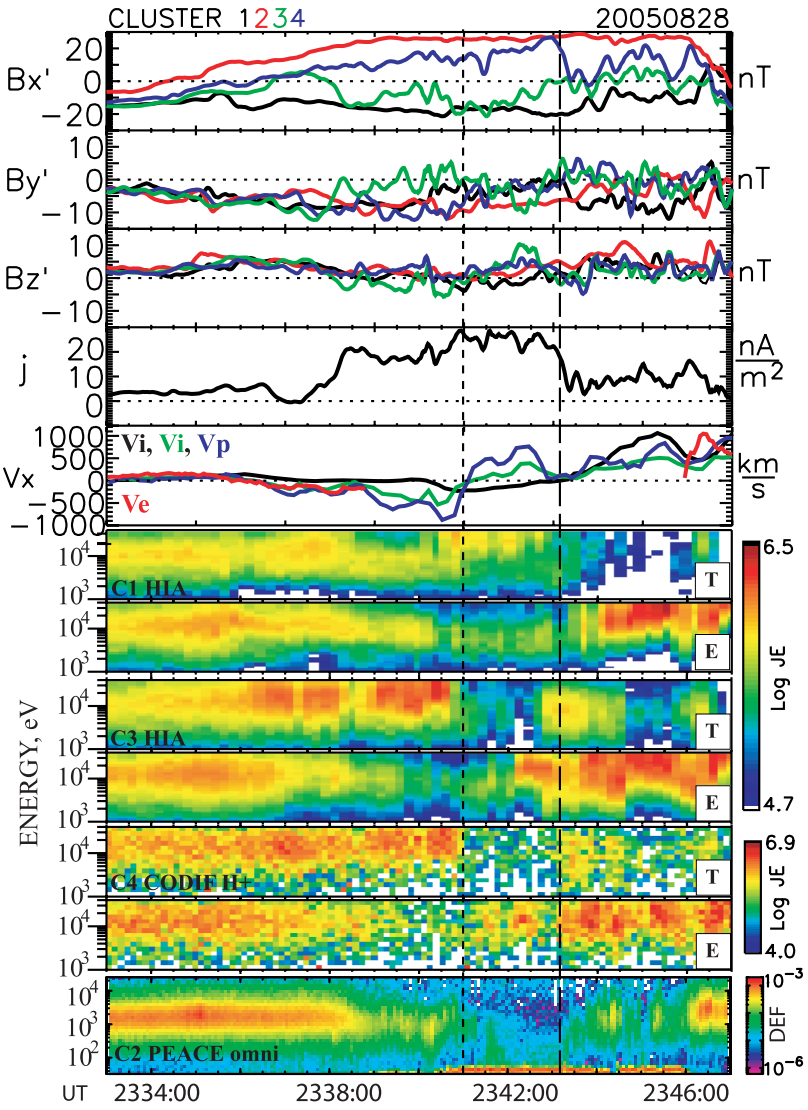

Figure 4. Cluster observations between 2333 and 2347 UT on 28 August 2005. (top to bottom) Components of the magnetic field form Cluster/FGM at all four spacecraft in the corrected GSM system; the the cross-tail current density, calculated from B_x at C3 and C4, separated by $Z_{34} \sim 900$ km; the X component of the ion bulk velocity from Cluster/CIS at C1, C3 (HIA), and C4 (CODIF) and the X component of the electron bulk velocity at C2 (Plasma Electron And Current Experiment (PEACE)); energy-time spectra from CIS at C1, C3, and C4 for tailward ("T") and earthward ("E") streaming ions in the energy range 1–40 keV (logarithm of energy flux EJ in keV/(s cm^2 sr keV) is color-coded); and the omnidirectional electron energy-time spectrum from PEACE at C2 (differential energy flux DEF in ergs/(s cm^2 sr eV) is color-coded).

is perpendicular to the magnetic field and to $\mathbf{V} \times \mathbf{B}$, which gives the direction [−0.46, 0.86, 0.23]) obtained at C1 during 2341:46–2341:58 UT. After 2343:10 UT (long-dashed line), C1 detected the enhancement of earthward flux with energy increasing up to 10 keV. The bulk velocity at C1 reversed at this time from ∼−200 km/s to 900 km/s. During 2336–2343 UT (interval bounded by vertical dashed lines in Figure 4), the C3/C4 pair detected the earthward flow, while C1, about 1 R_E tailward and dawnward, detected the tailward flow. The simultaneous ion distribution function at C1 and C3 during this interval are shown in Figure 5 (top). At C3, the three-spin-averaged magnetic field is [−13.1, −6.7, 2.9] nT. The $V_\perp$ direction is [0.04, 0.33, 0.94].

[17] The electron velocity from PEACE at C2 was in good agreement with the ion velocities at C3 and C4 until 2338:30 UT (solid line), when C2 exited the plasma sheet. The electron tailward bulk flow onset was detected at about 2336 UT, simultaneously with that of the ion velocity at C3 and C4. C1 observed a similar variation about 1 min later. C2 stayed in PSBL and the northern lobe between 2338:30 and ∼2346:00 UT, and the electron bulk velocity cannot be calculated.

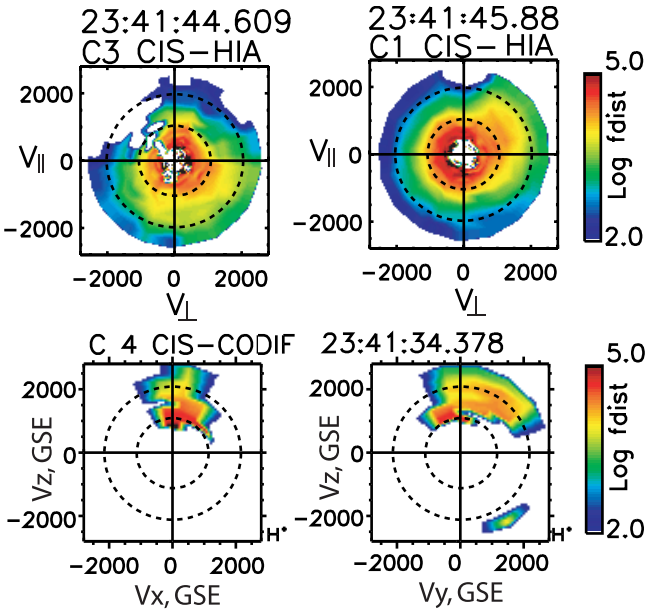

Figure 5. Three-spins accumulated ion distribution functions at C1 and C3 obtained during 2341:44–2341:56 UT in the ($V_{||}$, $V_{\perp}$) space (see text). (bottom) Six-spin accumulated proton distribution function from C4 CODIF obtained during 2341:34–2341:58 UT in the (V_x, V_z) and (V_y, V_z) GSE coordinates. The phase space density in s^3/km^6 is color coded.

[18] Figure 6 shows the 1 − s averaged magnetic field at C3 (gray curves) and C4 (black curves), the Y_{GSE} component of the convective electric field (E_{cy}), calculated from the magnetic field and velocity measurements at C3 and C4 (black), and the electric field measured by the Cluster Electric Field and Wave instrument (EFW) [*Gustafsson et al.*, 2001] at the same spacecraft (gray). The magnetic field data were smoothed by running average in a four-sample (1 spin) window. The vertical dashed line indicates the time of the flow reversal observed by C3 and C4.

[19] B_z at C3 reversed from southward to northward simultaneously with the bulk flow reversal from tailward to earthward, indicating the presence of an X line magnetic structure within the flow reversal. B_y at C3, on average, tends to change from positive during $V_x < 0$ to negative during $V_x > 0$. At C4, located in the northern halve of the current sheet, B_z was northward during $V_x < 0$ until 2340:20 UT, when a small-scale plasmoid passed by the spacecraft. $B_z \approx 0$ between 2340:20 and 2341 UT, and $B_z > 0$ during $V_x > 0$. B_y at C4, in average, reversed from negative to positive when the bulk velocity reversed from tailward to earthward. Although the average behavior of B_z (at C3) and B_y qualitatively agrees with the presence of the quadrupolar field structure in the vicinity of the X line, the quantitative analysis of the full resolution (22 vectors/s) shows that during the tailward flow only 27% of C3 ($B_x < 0$) samples fulfill the criterion $B_y > 0$, $B_z < 0$ and only 32% of C4 ($B_x > 0$) samples fulfill the criterion $B_y < 0$, $B_z < 0$. For the earthward flow, the observations are close to the pattern: 91% of C3 samples show $B_y < 0$ and $B_z > 0$, and 85% of C4 samples show $B_y > 0$ and $B_z > 0$.

[20] The convective electric field at C3 agrees well with E_y, obtained from the EFW instrument, at least in tendency. Both values were fluctuating around zero till ~2336 UT, experienced a negative excursion, corresponding to the tailward flow enhancement associated with $B_z > 0$, during 2336–2338 UT, and then increased up to 1–1.5 mV/m between 2338 and 2339:30 UT. The negative peaks of E_y and E_{cy}, observed at around 2340 UT, corresponds to a leading front of the small-scale plasmoid embedded into the tailward flow. At about 2340:30 UT, when $B_z < 0$ and $V_x < 0$, both E_y and E_{cy} increased up to about 3 mV/m. At the flow reversal, $E_y \approx E_{cy} \approx 2$ mV/m. This corresponds to an inflow velocity $V_z \approx 100$ km/s at $B_x = -20$, which is in agreement with CIS measurements. Starting at about 2340 UT, around the flow reversal time, the electric field displayed an impulsive behavior: both E_y and E_{cy} exhibit a set of simultaneous peak-like enhancements repeating with a period of 1 min (vertical bars in Figure 6). Similar behavior continues during the earthward flow (peaks at 2344, 2345:30 UT). The E_y peaks correspond to local maxima (minimum) of B_z. For C4, E_y and E_{cy} do not agree during 2339–2342 UT: E_{cy} at C4 is negative at around the flow reversal, between 2341:00 and 2342:00 UT, while E_y is positive. Since both B_z and V_x at C4 were positive during this interval, the negative E_{cy} was due to northward V_z. The northward ($V_z > 0$) streaming protons are indeed seen in the distributions shown in Figure 5 (bottom). This discrepancy between E_{cy} and E_y indicates decoupling between proton and magnetic field motion, i.e., violation of the frozen-in condition during this interval. Around the flow reversal, between 2340 and 2343 UT, E_y at C4 also exhibited the impulsive behavior, similar to that at C3. The $E_y > 0$ pulses are observed simultaneously in northern (C4) and southern (C3) parts of the current sheet. Thus, they correspond to an impulsive behavior of the tail-aligned magnetic field flux transfer, i.e., are temporal variations.

[21] To examine the normal electric field, we use the $\mathbf{E} \cdot \mathbf{B} = 0$ assumption. Calculating E_z (GSE) from EWF and FGM data, the criteria $|B_z| > 2$ nT and $|B_x/B_z| < 10$ are used (see, e.g., *Eastwood et al.* [2007] for details). The **E** vector with the calculated E_z was then used to calculate E_n. Figure 7 shows the results of these calculations for C3 (bottom) and C4 (top), located in southern and northern halves of the thin current sheet. Although the actual values of the calculated E_n (about −20 mV/m at C4 and about 5 mV/m at C3) may be not accurate, the tendency is clear: C4 in the northern half detects the negative E_n, while C3 in the southern halve detects mainly positive E_n within the boxed interval. Thus, the electric field, converging toward the thin sheet is observed around the bulk flow reversal instance and during the earthward flow. The normal components of the convective electric field at C3 and C4 (gray lines) are plotted to compare with the calculated E_n. At C3, E_n and $(\mathbf{V}_i \times \mathbf{B})_n$ are agreed in tendencies, while at C4 they exhibit different behavior.

[22] The ion pressure anisotropy is one of the key parameters defining the structure and stability of a TCS (see *Sitnov et al.* [2006] for a review). Figure 8 shows a temporal behavior of the ion (proton at C4) pressure tensor components parallel ($P_{||}$) and perpendicular ($P_{\perp 1}$ and $P_{\perp 2}$) to the instantaneous magnetic field at C3 and C4, situated in the southern and northern halves of the TCS, respectively.

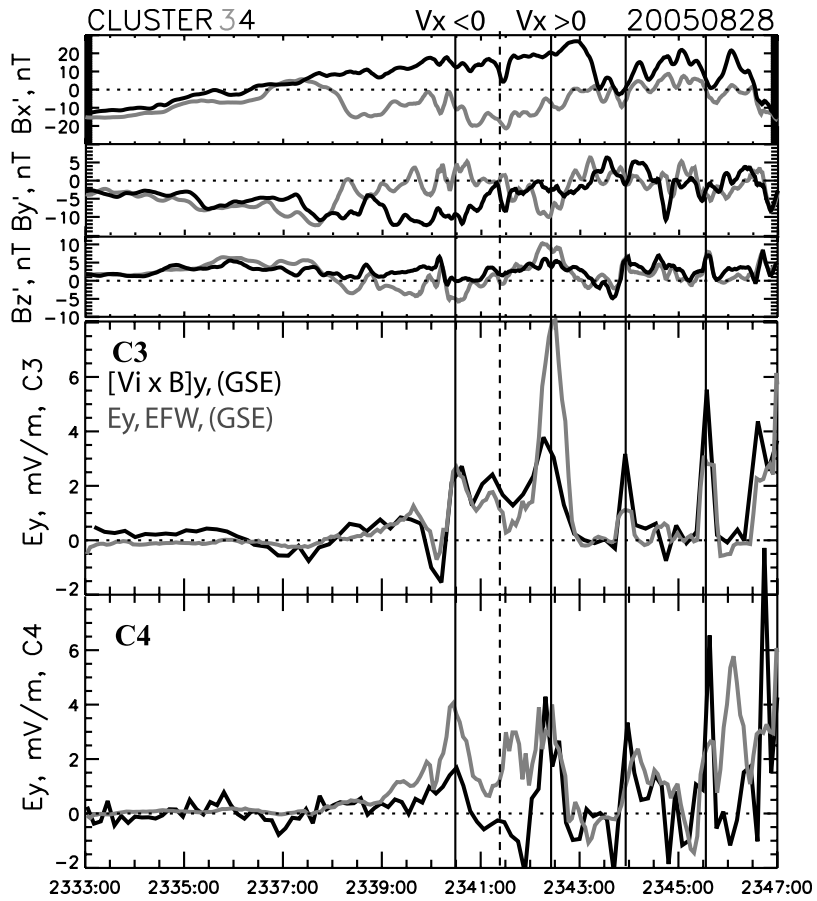

Figure 6. (top to bottom) X and Z components of the magnetic field at C3 (gray) and C4 (black) and the Y_{GSE} component of the convective electric field $\mathbf{E}_c = -\mathbf{V} \times \mathbf{B}$ (black) and the correspondent component of the electric field, obtained from Cluster/EFW instrument (gray) at C3 and C4 versus UT during 2333–2347 UT. The vertical dashed line indicates the bulk flow reversal time.

At both probes $P_{\|} > P_{\perp}$ ($P_{\perp} = 0.5(P_{\perp 1} + P_{\perp 2})$) between ~2339 and ~2341 UT, indicating a cigar-type anisotropy during the tailward bulk flow in the TCS. During the ~1-min-long interval just after the flow reversal (2341:10–2342:10 UT), the pressure anisotropy changed to the pancake-like ($T_{\|} < T_{\perp}$) one. After ~2342:10 UT the pressure at C4 became rather isotropic, while C3 showed rather cigar-like anisotropy. Note a change in ion and proton populations at about 2343 UT, visible in the ET spectra (Figure 4). Since $P_{\perp 1} \approx P_{\perp 2}$, the pressure in the observed TCS is gyrotropic. The cigar-type anisotropy $P_{\|} - P_{\perp} < \mu_0^{-1} B_0^2$, where $B_0 = 25$ nT is the magnetic field in the lobe, measured by C2. Thus, the TCS is stable with respect to the fire hose instability [*Treumann and Baumjohann*, 1997].

[23] Figure 9 shows omnidirectional electron fluxes at C3 and C4 near the flow reversal (indicated by vertical line). During 2340:45–2342:10, C3 detected a decrease of the electron flux with some decrease of electron energy. Contrary, at the same time, C4 showed an increase of electron energy from 1 keV to ~3 keV.

4. Discussion

[24] Timing analysis of the magnetic field and bulk velocity (ion and electron) at all four spacecraft shows that Cluster entered into the bulk flow reversal region from the dawn side with a velocity of 50 km/s. Thus, Cluster detected a slow dawnward expansion of the localized active region. This dawnward expansion is consistent with auroral data

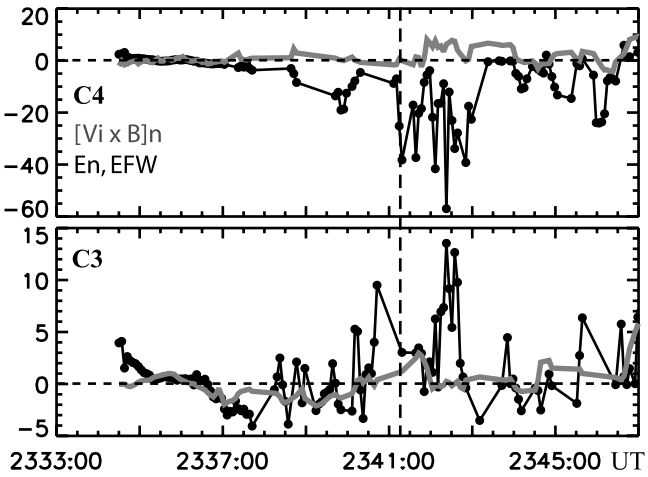

Figure 7. Time series of the normal electric field component E_n at (top) C4 and (bottom) C3. See details of the E_n calculation in text.

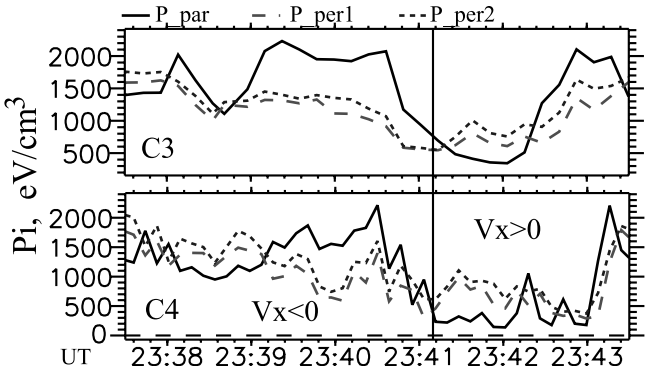

Figure 8. Evolution of the ion (C3) and proton (C4) pressure tensor components $P_{||}$, $P_{\perp 1}$, and $P_{\perp 2}$ within the thin current sheet with tailward ($V_x < 0$) to earthward ($V_x > 0$) flow reversal during 2337:30–2343:30 UT. The vertical line indicates the time of the bulk flow reversal.

obtained by the IMAGE satellite: the auroral activation, visible at the snapshot at 2339:28 UT (Figure 1) is duskward of the Cluster foot point. It expands in longitude during the substorm development, covering the region of the Cluster foot points, as seen in the next two images.

[25] The ion bulk flow reversal was detected by three of the four spacecraft in the plasma sheet during the current sheet thinning. The flow reversal was detected first by C3/C4 pair, then, about 2 minutes later, by C1. During about 2 min the earthward probes (C3 and C4) detected the earthward bulk flow ($V_x \approx 800$ km/s) simultaneously with the northward B_z, while the tailward one, separated by approximately 1.5 R_E, (C1) detected the tailward bulk flow with smaller velocity ($V_x \approx 300$ km/s) and the southward B_z. Thus, the C3/C4 pair and C1 were situated earthward and tailward of the flow reversal line, i.e., X line in the framework of magnetic reconnection, respectively. It should be noted, however, that the observations are not fully consistent with the simple X line pattern: B_z, observed by C4 during the tailward flow was northward (see Figure 4), contrary to expectation, while C3, separated by a couple of ion inertial length, observed $B_z < 0$, which agrees with the X line model. The difference in B_z at C3 and C4 during the tailward flow (2339–2341 UT) may be explained supposing a long magnetic island embedded into the tailward flow. Such structures were observed near reconnection site [e.g., *Nakamura et al.*, 2006; *Eastwood et al.*, 2007], and appeared in PIC simulations [e.g., *Divin et al.*, 2007].

[26] An important point of this case study is about violations of the frozen-in condition in a TCS. At one probe (C3) the comparison of the convection electric field $\mathbf{E}_c = -\mathbf{V} \times \mathbf{B}$, calculated using CIS and FGM data and double probe measurements gives good agreement in tendency: maxima of E_{ey} coincide with those of the measured E_y (Figure 6). At the other probe (C4) the remarkable disagreements were detected during about two minutes around the flow reversal, when $E_y > 0$ but $E_c < 0$. Normal components of the double probe and convective electric fields also strongly differ at that time. The spacecraft were separated by about 900 km, which is about two ion inertial lengths (460 km for $N = 0.25$ cm^{-3}), and situated in southern and northern halves of the TCS. Again, interpreting the observation in the framework of magnetic reconnection, it is likely that C4 entered an ion diffusion region near the flow reversal, where ions are decoupled from the magnetic field, while C3 stays away of the diffusion region, showing $\mathbf{E} \approx -\mathbf{V} \times \mathbf{B}$ most of the time. Electron spectra at C3 and C4 (Figure 9) also show that C4 is in a region of electron energization [cf. *Imada et al.*, 2007], while C3 is mainly out of this region. Thus, the region of nonfrozen-in flux is limited in space by, at least, 900 km (less than the estimate obtained by *Lui et al.* [2007]).

[27] Note that although frozen-in condition was roughly satisfied, C3 observed signatures of the quadrupolar magnetic field. The normal electric field, calculated from the double probe measurements, qualitatively agrees with the normal component of the convective electric field, except for the aforementioned short peak. Thus, in this case the quadrupolar magnetic field cannot be attributed to the Hall effect directly, since the Hall currents may exist only inside the ion diffusion region, where ions are unmagnetized. However, a quadrupolar structure may exist also away from the diffusion region because of field-aligned currents, closing electron currents in the Hall zone [*Fujimoto et al.*, 2001; *Nakamura et al.*, 2004; *Alexeev et al.*, 2005; *Treumann et al.*, 2006]. The quadrupolar magnetic field, observed near the flow reversal by C4, may be attributed to the Hall effect:

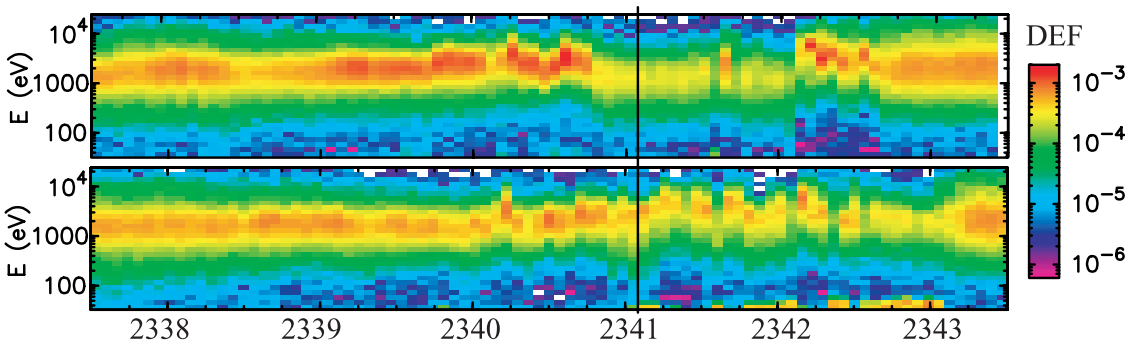

Figure 9. Omnidirectional electron energy-time spectra, obtained by PEACE at C3 and C4 near the bulk flow reversal. The vertical line indicates the time of the tailward to earthward flow reversal. Differential energy flux (DEF) is color coded.

the normal electric field strongly deviates from $[-\mathbf{V} \times \mathbf{B}]_n$ indicates ion-magnetic field decoupling.

[28] The important observation is the impulsive behavior of the magnetic flux transfer: E_{cy} as well as E_y exhibits temporal spikes with amplitudes of 4–6 mV/m, recurrent at 60–90 s. These electric field pulses were detected by both spacecraft, situated on the opposite sides of the thin current sheet. Since both probes detected the positive E_y during these pulses, this electric field modulation is not due to plasma sheet flapping. Thus, the impulsive behavior of the electric field indicates that the process of plasma acceleration at the flow reversal is time-dependent. The impulsive activations with the characteristic timescale of 1–2 min are common for magnetotail dynamics, and have been detected in spacecraft observations in the plasma sheet [e.g., *Angelopoulos et al.*, 1992; *Schödel et al.*, 2001] as well as in auroral and ground-based magnetic observations (see *Sergeev et al.* [1996] for a review). It is supposed that spatially localized impulsive dissipation events [*Sergeev et al.*, 1996] with the timescale of 1 min are elementary building blocks of magnetospheric activity. It is likely, and our observations support it, these pulses are generated by some plasma instability (or instabilities) generated in a TCS.

[29] The impulsive behavior of the electric field is predicted by some theoretical models of transient reconnection [e.g., *Semenov et al.*, 2005] and models including secondary tearing and coalescence instability [*Ma and Bhattacharjee*, 1999]. Recent kinetic simulations of undriven magnetic reconnection with open boundary conditions also show impulsive electric field near X line with a duration of the pulses of $\sim$50 Ω_{ci} ($\approx$300 s for B = 10 nT) [*Daughton et al.*, 2006]. It was pointed, that peaks of the electric field are associated with secondary magnetic islands formation in a stretched diffusion region. Between the peaks, the electric field decreases down to $\approx$0.5 of the peak value. Similar behavior of the electric field was observed near flow reversal, between 2340:30 and 2343:00 UT (Figure 6). The bipolar B_z variation may be interpreted as the signature of the secondary magnetic island [see also *Nakamura et al.*, 2006; *Eastwood et al.*, 2007].

[30] Impulsive activations with the characteristic time of 50–100 s may also result from the ballooning-type instability of TCSs [e.g., *Bhattacharjee et al.*, 1998]. It was shown that because of 3-D full particle simulations, the ballooning mode becomes unstable when the ratio of the magnetic field curvature radius and the proton gyroradius is about 0.1 [*Pritchett and Coronoti*, 1999]. The bulk flow produced by the ballooning mode is predicted to be of 200 km/s or less, which is smaller, than the observed bulk flow velocity. The magnetic field and plasma pressure variations due to the ballooning instability, are predicted to be rapidly propagating in cross-tail direction ($k_y \gg (k_x, k_z)$). Observations in the near-Earth magnetotail showed the duskward propagation of the magnetic field and ion flux variations at the velocity of 200 km/s [*Chen et al.*, 2003]. As mentioned above, we found rapid tailward and very slow dawnward propagation of plasma and magnetic field variations. Thus, the observed electric field pulses may hardly be explained in the frame of the ballooning-based current disruption scenario. However, more detailed analysis of the magnetic field fluctuations is needed to draw a decisive conclusion.

5. Conclusions

[31] We have examined multipoint observations of active magnetotail plasma sheet during a transition between growth and expansion phases of a substorm, provided by the Cluster spacecraft. It was found that the the activity starts in the spatially localized region near midnight meridian, duskward of the Cluster foot point. The active region expanded dawnward during the substorm.

[32] A thin current sheet with the half thickness of $\sim 2c/\omega_{pi}$ and a current density exceeding 30nA/m^2, followed by high-speed flow with fluctuating magnetic field, was observed by Cluster at $X \sim -17$ R$_E$, during $\sim$5 min at around the substorm onset. Plasma bulk flow reversal from tailward to earthward was detected during this interval. The analysis of Cluster observations in the thin current sheet with the flow reversal show signatures of the ion diffusion region, passing the spacecraft. Using a pair of spacecraft, the vertical scale of the ion diffusion region was estimated to be less than 900 km.

[33] The observations showed impulsive activations of the magnetic flux transfer in the thin current sheet with the timescale of about 1 min. Two spacecraft within the thin current sheet observed transient enhancements of the electric field simultaneously, which is telling that it is a temporal but not spatial behavior.

[34] Models of impulsive (transient) reconnection provide a reasonable framework to interpret these observations; however, the observations reveal remarkable disagreements with the classical 2.5-D reconnection pattern.

[35] **Acknowledgments.** We thank H.-U. Eichelberger, G. Laky, S. Schwartz, C. Mouikis, L. Kistler, E. Georgescu, and E. Penou for help with data and software and V. Angelopoulos for fruitful discussion. We acknowledge the Cluster Active Archive and CDAWeb for providing Cluster-EFW and WIND data used in this study. This work was fruitfully discussed by EUROPLANET 3 Cluster-GBO coordination workshops and by Cluster Tail workshops.

[36] Amitava Bhattacharjee thanks Kevin Quest and another reviewer for their assistance in evaluating this paper.

References

Alexeev, I. V., C. J. Owen, A. N. Fazakerley, A. Runov, J. P. Dewhurst, A. Balogh, H. Rème, B. Klecker, and L. Kistler (2005), Cluster observations of currents in the plasma sheet during reconnection, *Geophys. Res. Lett.*, *32*, L03101, doi:10.1029/2004GL021420.

Angelopoulos, V., W. Baumjohann, C. F. Kennel, F. V. Coroniti, M. G. Kivelson, R. Pellat, R. J. Walker, H. Lühr, and G. Paschmann (1992), Bursty bulk flows in the inner central plasma sheet, *J. Geophys. Res.*, *97*, 4027–4039.

Asano, Y., T. Mukai, M. Hoshino, Y. Saito, H. Hayakawa, and T. Nagai (2004), Statistical study of thin current sheet evolution around substorm onset, *J. Geophys. Res.*, *109*, A05213, doi:10.1029/2004JA010413.

Balogh, A., et al. (2001), The Cluster magnetic field investigation: Overview of in-flight perfomance and initial results, *Ann. Geophys.*, *19*, 1207–1217.

Baumjohann, W., and R. A. Treumann (1996), *Basic Space Plasma Physiscs*, 329 pp., Imperial Coll. Press, London.

Baumjohann, W., et al. (2007), Dynamics of thin current sheets: Cluster observations, *Ann. Geophys.*, *25*, 1365–1389.

Bhattacharjee, A., Z. W. Ma, and X. Wang (1998), Ballooning instability of a thin current sheet in the high-Lundquist-number magnetotail, *Geophys. Res. Lett.*, *25*, 861–864.

Birn, J., and E. R. Priest (Eds.) (2007), *Reconnection of Magnetic Fields*, Cambridge Univ. Press, Cambridge, U. K.

Borg, A. L., M. Øieroset, T. D. Phan, F. S. Mozer, A. Pedersen, C. Mouikis, J. P. McFadden, C. Twitty, A. Balogh, and H. Rème (2005), Cluster en-

counter of a magnetic reconnection diffusion region in the near-Earth magnetotail on September 19, 2003, *Geophys. Res. Lett.*, *32*, L19105, doi:10.1029/2005GL023794.

Chen, L.-J., A. Bhattacharjee, K. Sigsbee, G. Parks, M. Fillingim, and R. Lin (2003), Wind observations pertaining to current disruption and ballooning instability during substorms, *Geophys. Res. Lett.*, *30*(6), 1335, doi:10.1029/2002GL016317.

Daughton, W., J. Scudder, and H. Karimabadi (2006), Fully kinetic simulations of undriven magnetic reconnection with open boundary conditions, *Phys. Plasmas*, *13*, 072101, doi:10.1063/1.2218817.

Divin, A. V., M. I. Sitnov, M. Swisdak, and J. F. Drake (2007), Reconnection onset in the magnetotail: Particle simulations with open boundary conditions, *Geophys. Res. Lett.*, *34*, L09109, doi:10.1029/2007GL029292.

Eastwood, J. P., et al. (2007), Multi-point observations of the Hall electromagnetic field and secondary island formation during magnetic reconnection, *J. Geophys. Res.*, *112*, A06235, doi:10.1029/2006JA012158.

Fujimoto, M., T. Nagai, N. Yokokawa, Y. Yamade, T. Mukai, Y. Saito, and S. Kokubun (2001), Tailward electrons at the lobe-plasma sheet interface detected upon dipolarizations, *J. Geophys. Res.*, *106*, 21,255–21,262.

Gustafsson, G., et al. (2001), First results of electric field and density observations by CLUSTER EFW based on initial months of operation, *Ann. Geophys.*, *19*, 1219–1240.

Imada, S., R. Nakamura, P. W. Daly, M. Hoshino, W. Baumjohann, S. Mühlbachler, A. Balogh, and H. Rème (2007), Energetic electron acceleration in the downstream reconnection outflow region, *J. Geophys. Res.*, *112*, A03202, doi:10.1029/2006JA011847.

Johnstone, A. D., et al. (1997), PEACE: A plasma electron and current experiment, *Space Sci. Rev.*, *79*, 351–398.

Lui, A. T. Y. (1996), Current disruption in the Earth's magnetosphere: Observations and models, *J. Geophys. Res.*, *101*, 13,067–13,088.

Lui, A. T. Y., et al. (2006), Cluster observation of plasma flow reversal in the magnetotail during a substorm, *Ann. Geophys.*, *24*, 2005–2013.

Lui, A. T. Y., Y. Zheng, H. Rème, M. W. Dunlop, G. Gustafsson, and C. J. Owen (2007), Breakdown of the frozen-in condition in the Earth's magnetotail, *J. Geophys. Res.*, *112*, A04215, doi:10.1029/2006JA012000.

Ma, Z. W., and A. Bhattacharjee (1999), Sudden disruption of a thin current sheet in collisionless Hall magnetohydrodynamics due to secondary tearing and coalescence instabilities, *Geophys. Res. Lett.*, *26*, 3340–3367.

Nagai, T., et al. (1998), Structure and dynamics of magnetic reconnection for substorm onsets with Geotail observations, *J. Geophys. Res.*, *103*, 4419–4440.

Nagai, T., I. Shinohara, M. Fujimoto, S. Machida, R. Nakamura, Y. Saito, and T. Mukai (2003), Structure of the Hall current system in the vicinity of the magnetic reconnection site, *J. Geophys. Res.*, *108*(A10), 1357, doi:10.1029/2003JA009900.

Nakamura, R., et al. (2002), Fast flow during current sheet thinning, *Geophys. Res. Lett.*, *29*(23), 2140, doi:10.1029/2002GL016200.

Nakamura, R., et al. (2004), Flow shear near the boundary of the plasma sheet observed by Cluster and Geotail, *J. Geophys. Res.*, *109*, A05204, doi:10.1029/2003JA010174.

Nakamura, R., et al. (2006), Dynamics of thin current sheets associated with magnetotail reconnection, *J. Geophys. Res.*, *111*, A11206, doi:10.1029/2006JA011706.

Oieroset, M., T. D. Phan, M. Fujimoto, R. P. Lin, and R. P. Lepping (2001), In situ detection of collisionless reconnection in the Earth's magnetotail, *Nature*, *412*, 414–417.

Pellinen, R. J., W. Baumjohann, W. J. Heikkila, V. A. Sergeev, A. G. Yahnin, G. Marklund, and A. O. Melnikov (1982), Event study on presubstorm phases and their relation on the energy coupling between solar wind and magnetosphere, *Planet. Space Sci.*, *30*, 371–388.

Pritchett, P. L., and F. V. Coronoti (1999), Drift ballooning mode in a kinetic model of the near-Earth plasma sheet, *J. Geophys. Res.*, *104*, 12,289–12,299.

Rème, H., et al. (2001), First multispacecraft ion measurements in and near the Earth's magnetosphere with the identical Cluster ion spectrometry (CIS) experiment, *Ann. Geophys*, *19*, 1303–1354.

Roux, A., et al. (1991), Plasma sheet instability related to the westward traveling surge, *J. Geophys. Res.*, *96*, 17,697–17,714.

Runov, A., et al. (2003), Current sheet structure near magnetic X-line observed by Cluster, *Geophys. Res. Lett.*, *30*(11), 1579, doi:10.1029/2002GL016730.

Schödel, R., W. Baumjohann, R. Nakamura, V. A. Sergeev, and T. Mukai (2001), Rapid flux transport in the central plasma sheet, *J. Geophys. Res.*, *106*, 301–313.

Semenov, V. S., T. Penz, V. V. Ivanova, V. A. Sergeev, H. K. Biernat, R. Nakamura, M. F. Heyn, I. V. Kubyshkin, and I. B. Ivanov (2005), Reconstruction of the reconnection rate from cluster reasurements: First results, *J. Geophys. Res.*, *110*, A11217, doi:10.1029/2005JA011181.

Sergeev, V. A., T. I. Pulkkinen, and R. J. Pellinen (1996), Coupled-mode scenario for the magnetospheric dynamics, *J. Geophys. Res.*, *101*, 13,047–13,065.

Sergeev, V., et al. (2007), Observation of repeated intense near-Earth reconnection on closed field lines with Cluster, Double Star, and other spacecraft, *Geophys. Res. Lett.*, *34*, L02103, doi:10.1029/2006GL028452.

Sitnov, M. I., M. Swisdak, P. N. Guzdar, and A. Runov (2006), Structure and dynamics of a new class of thin current sheets, *J. Geophys. Res.*, *111*, A08204, doi:10.1029/2005JA011517.

Sonnerup, B. U. Ø. (1979), *Solar System Plasma Physics*, vol. III, 45 pp., North-Holland, New York.

Treumann, R. A., and W. Baumjohann (1997), *Advanced Space Plasma Physiscs*, 381 pp., Imperial Coll. Press, London.

Treumann, R. A., C. H. Jaroschek, R. Nakamura, A. Runov, and M. Scholer (2006), The role of the Hall effect in collisionless magnetic reconnection, *Adv. Space. Res.*, *38*, 101–111.

Tsyganenko, N. A. (1995), Modeling the Earth's magnetospheric magnetic field confined within a realistic magnetopause, *J. Geophys. Res.*, *100*, 5599–5612.

Vaivads, A., Y. Khotyaintsev, M. André, A. Retinò, S. C. Buchert, B. N. Rogers, P. Décréau, G. Paschmann, and T. D. Phan (2004), Structure of the magnetic reconnection diffusion region from four-spacecraft observations, *Phys. Rev. Lett.*, *93*(10), 105001, doi:10.1103/PhysRevLett.93.105001.

Wilber, M., et al. (2004), Cluster observations of velocity space-restricted ion distributions near the plasma sheet, *Geophys. Res. Lett.*, *31*, L24802, doi:10.1029/2004GL020265.

Wygant, J. R., et al. (2005), Cluster observations of an intense normal component of the electric field at a thin reconnecting current sheet in the tail and its role in the shock-like acceleration of the ion fluid into the separatrix region, *J. Geophys. Res.*, *110*, A09206, doi:10.1029/2004JA010708.

I. Alexeev, A. N. Fazakerley, and C. J. Owen, Mullard Space Science Laboratory, University College London, Dorking RH5 6NT, UK.

O. Amm, Finnish Meteorological Institute, FIN-00101 Helsinki, Finland.

M. André and A. Vaivads, Swedish Institute of Space Physics, SE-75121 Uppsala, Sweden.

W. Baumjohann and R. Nakamura, Space Research Institute, Austrian Academy of Sciences, A-8042 Graz, Austria.

I. Dandouras, CESR/CNRS, CEDEX 4, F-31028 Toulouse, France.

H. Frey, Space Sciences Laboratory, University of California, Berkeley, CA 94720-7450, USA.

B. Klecker, Max Planck Institute, D-85748 Garching, Germany.

E. Lucek, Space and Atmospheric Physics Group, Blackett Laboratory, Imperial College, London SW7 2AZ UK.

A. Runov, Institute of Geophysics and Planetary Physics, UCLA, 3845 Slichter Hall, Los Angeles, CA 90095, USA. (arunov@igpp. ucla.edu)

V. A. Sergeev, Institute of Physics, St. Petersburg State University, St. Petersburg 198504, Russia.